ATD: a multiplatform for semiautomatic 3-D detection of kidneys and their pathology in real time

Article

Accepted Version

It is advisable to refer to the publisher's version if you intend to cite from the work. See [Guidance on citing](#).

Automatic Tumour Detector: A multi-platform for 3D automatic detection of abdominal pathology based on features extraction

Emmanouil Skounakis[1], Konstantinos Banitsas[1], Atta Badii[2],
Stavros Tzoulakis[3], Emmanuel Maravelakis[4] and Antonios Konstantaras[4]

[1] School of Engineering and Design, Dep. of E&CE, Brunel University, West London, UK
[2] Intelligent Systems Research Laboratory, School of Systems Engineering, University of Reading, Reading, UK
[3] Venizeleio & Pananio General Hospital, Urology Department, Heraklion, Crete, Greece
[4] Technological Educational Institute of Crete, Chania, Crete, Greece

Abstract— This research presents a novel multi-functional system for medical Imaging-enabled Assistive Diagnosis (IAD). Although the IAD demonstrator has focused on abdominal images and supports the clinical diagnosis of kidneys using CT/MRI imaging, it can be adapted to work on image delineation, annotation and 3D real-size volumetric modelling of other organ structures such as the brain, spine, etc. The IAD provides advanced real-time 3D visualisation and measurements with fully automated functionalities as developed in two stages. In the first stage, via the clinically driven user interface, specialist clinicians use CT/MRI imaging datasets to accurately delineate and annotate the kidneys and their possible abnormalities, thus creating "3D Golden Standard Models". Based on these models, in the second stage, clinical support staff i.e. medical technicians interactively define model-based rules and parameters for the integrated "Automatic Recognition Framework" to achieve results which are closest to that of the clinicians. These specific rules and parameters are stored in "Templates" and can later be used by any clinician to automatically identify organ structures i.e. kidneys and their possible abnormalities. The system also supports the transmission of these "Templates" to another expert for a second opinion. A 3D model of the body, the organs and their possible pathology with real metrics is also integrated. The automatic functionality was tested on eleven MRI datasets (comprising of 286 images) and the 3D models were validated by comparing them with the metrics from the corresponding "3D Golden Standard Models". The system provides metrics for the evaluation of the results, in terms of Accuracy, Precision, Sensitivity, Specificity and Dice Similarity Coefficient (DSC) so as to enable benchmarking of its performance. The first IAD prototype has produced promising results as its performance accuracy based on the most widely deployed evaluation metric, DSC, yields 97% for the recognition of kidneys and 96% for their abnormalities; whilst across all the above evaluation metrics its performance ranges between 96% and 100%. Further development of the IAD system is in progress to extend and evaluate its clinical diagnostic support capability through development and integration of additional algorithms to offer fully computer-aided identification of other organs and their abnormalities based on CT/MRI/Ultra-sound Imaging.

Keywords: 3D Medical Image Segmentation, Fully Automatic Segmentation, Medical Image Analysis, Abdominal Imaging, Virtualisation of the Human Physiology, Computer Aided Diagnosis, Virtual Biopsy

1 INTRODUCTION

THE rapid evolution of advanced medical image modalities such as the modern Magnetic Resonance Imaging (MRI) scanners and the huge amount of data provided, has brought about the need for more automated processes in the field of computer-aided diagnosis. Clinicians need to examine large numbers of slices of MRI datasets to detect abnormalities; which is a difficult and time consuming task due to the complexity of medical images. As efficient processing and analysis of the

images is the key to making accurate and timely diagnosis feasible, there is a clear need for systems that will automatically detect organs and their possible abnormalities and provide real metrics.

Currently, the diagnosis of kidney abnormalities is performed by doctors without the aid of computers. Nevertheless, the development of automatic detection systems as a first step towards supporting a more efficient and effective clinical diagnosis process is very challenging and requires close collaboration between renal clinicians and medical technicians.

To date, we can find several attempts aimed at improving the abdominal image segmentation process. Park et al. (2003) have computed a mean image from hand-segmented CT abdominal scans. Their registration process involves thin plate splines for the propagation of the segmentation of the liver, kidneys and aorta. Similarly, data from probabilistic atlases has been used by Shimizu et al. (2006) and Yao et al. (2006) to segment abdominal images. Measures of relationship and hierarchy between organs and manual landmarks have been used in both systems. Hu et al. (2004) have used Multi-dimensional CT data for an independent component analysis in a variational Bayesian mixture. Sakashita et al. (2007) have segmented abdominal CT images based on expectation-maximisation theory and principal component analysis.

Recently, several sophisticated algorithms have been devised for more accurate automatic detection of kidneys. Kim and Park (2004) have used a grey-level threshold method to segment the kidney and a region-growing process to segment kidney tumours with a sensitivity of 85%. Rao et al. (2005) have achieved a mean volume overlap of 88.8% for kidneys with m-rep models based on manual segmentations from a collection of images that did not include the targets. Lin et al. (2006) have achieved a Dice Similarity Coefficient (DSC) of 88% between automatic and manual segmentation. They have extracted the kidney region based on the statistical geometric location of the kidney within the abdomen and on a series of image processing operations. A Framework for a fully automatic grey-level based segmentation of kidneys that employs a fast matching technique is presented by Campadelli et al. (2008) with a similarity volume overlap of 95%. Li and Fei (2008) have proposed a 3D minimal path segmentation method with an average overlap ratio of 93%. Chen et al. (2011) have presented a finite element method (FEM) based 3D tumour growth prediction for kidney tumours, with an average true positive fraction of 91.4% on all tumours. Prevost et al. (2012) have automatically localised the kidney with a novel ellipsoid detector and then applied deformation of this ellipsoid with a model-based approach in the segmentation process. In their case, Ultrasound Images were used to yield a DSC of 87.5%. Gloger et al. (2012) have deployed Bayesian concepts for a probability map generation to achieve an automatic kidney Parenchyma volumetry with a DSC of 90.3%. Finally, Akbari and Fei (2012) have presented a combination of texture features and a statistical matching of geometrical shape of kidneys, for an automatic segmentation in 3D MRI images with a mean DSC of 90.6%. It must also be noted that although all the above mentioned methods detect kidneys, only Kim and Park (2004) and Chen et al. (2011) detect tumours as well.

Compared to the methods mentioned above, the proposed "Automatic Segmentation Framework" integrated in the ATD platform, yields a higher mean DSC of 97% for the recognition of kidneys and 96% for their abnormalities (Tumours, Stones and Cysts).

In an effort to develop a user friendly environment to support the clinician without requiring any knowledge of medical image processing, we have also developed the Automatic Tumour Detector (ATD). It is a new, easy-to-use platform supporting multi-colour objects annotations resulting in a fully automated identification method of kidneys and any of their pathologies (tumours, stones and cysts) as well as a 3D multi-modal interactive visualisation environment. The development of this system has been clinically driven, providing the clinicians with useful visual information and real metrics of the detected areas. The advantages of this platform include rapid processing of CT/MRI

datasets on a large scale, easy and accurate delineation of highly complex medical images, an easy-to-handle multi-functional annotation system and a fully automatic framework for the recognition of kidneys and their structural anomalies/pathologies. Moreover, it allows the storage of the information in small anonymous external files to ensure their fast transmission via networks to other computers or mobile devices. The user also has the option to send a "Template" file to a second radiologist to get a second opinion about the findings. This is a first step towards the implementation of a complete telemedical application for mobile clinicians.

The rest of this paper is organised as follows: Section 2 provides a brief overview of the Graphical User Interface (GUI) of the platform; summarising its main functions. Section 3 elaborates on the internal processes used to extract information from the available datasets while section 4 focuses in more detail on the construction of the filters used to support these processes. Section 5 reports on the performance evaluation of the system and results while section 6 provides the analysis of the evaluation results and section 7 presents the conclusion and sets out the future work as planned and in progress.

2   MATERIAL AND METHODS

2.1   Platform design

The platform development was based on the .NET Framework architecture (Benefits of the Microsoft .NET Framework, 2012), so that it could be deployed in any Windows-based computer with the .NET Framework version 4.0 or later versions. However, given that the system uses the Mono project functionality and libraries (The Mono Project, 2012), the user can run the application in many other Linux-based environments through the No-Touch Deployment (Benefits of the Microsoft .NET Framework, 2012). The user-interface design is clinically-led and its features follow the Windows 8 layout (i.e. the Metro Design, already applied on windows-based smart phones).

Fig. 2.1: Platform Design. The clinician has finished the segmentation task on slide no. 12. The Segments panel on the right side contains the delineated regions of interest (Left Kidney, Right Kidney and Right Kidney Tumour)

3

2.2   Importing Medical Images

The user can introduce any number of DICOM images into the platform. These images will appear as thumbnails at the bottom of the screen, below the enlarged selected image (Fig. 2.1). A system of axes allows the adjustment of the "Window level" and "Window width" values which enable the user to adjust the "Brightness" and the "Contrast" of the image. "Window Width" is the difference between the brightest and dullest pixel value and "Window Level" is the mid-value between the brightest and dullest pixel value. The "zoom-in/zoom-out" options and the "hand" tool allow the user to adjust the size and the position of the selected image on the screen so as to be able to focus on specific sections of the image for more detailed examination.

2.3   Manual Segmentation Panel

This panel integrates an advanced implementation of the "Region-Growing" segmentation algorithm (top-left corner of Fig. 2.1). This semi-automatic segmentation method is to assist the clinician in rapidly defining the regions of interest in the image. Boundary refinement can be achieved by using the "Pencil" and "Eraser" tools allowing for the expansion or shrinkage of the selected areas so as to add or remove any mistakenly selected or ignored pixels. At the end of this process, the "Segments" panel on the right side of the platform contains the user-defined labels corresponding to the selected areas. This acts essentially as a clinical examination dashboard.

2.4   A Multi-functional Annotation system

The integrated multi-functional annotation system facilitates the delineation of areas of interest in the selected image. These areas can be labelled, coloured, renamed or deleted as depicted in Fig. 2.1. When the user clicks on the "Add" button in the "Segments" panel, the "Annotation Selection" window appears. This allows the user to select "thumbnail" images in order to add annotations either by choosing from a list of already existing labels, or by typing in a new label. The process can be applied to a single image or to a number of images simultaneously. The user can select any of the images to delineate and colour an area of interest by using either the manual or the automatic segmentation methods from the "Framework" panel.

Any such designated labels that may have been assigned as annotations for a single or group of images can be modified through the "Re-name" button. The user can also select and delete any annotations by pressing the "Remove" button.

2.5   Automatic Segmentation Panel

The Framework is based mainly on a region-oriented segmentation method (Bassman and Besslich, 1995) for automatic identification of organs and their possible structural abnormalities/pathologies such as cysts, stones and tumours. A panel enables the clinician to interactively adjust the parameters used in this method and check the corresponding results in real-time. The clinician can perform preliminary checks to help select the imaging parameters experimentally in a single slide. Once the result is acceptable, the parameters and the rules can be applied automatically to the entire image dataset and can be saved in a "Template" with a name that corresponds to the (sub) area identified (e.g. kidney, right or left). For highly complex images, the clinician also has the option of using a Region of Interest (ROI) focusing technique by defining a "working area" where the Framework will be applied.

2.6   Validation Panel

To check accuracy and precision, the result from the "Automatic Segmentation" process (Section 2.5) can be compared to the semi-automatic result of the clinician's output (Section 2.3).

This can be achieved by means of comparison of the resulting 3D Volume models (clinician's Golden Standard model versus the medical technician's Volume model) by using the metrics from the "3D Rendering" process (Section 2.7).

Alternatively, the "Validation" panel allows a more precise evaluation by comparing the results for every single slide between the two models (Fig. 2.2).
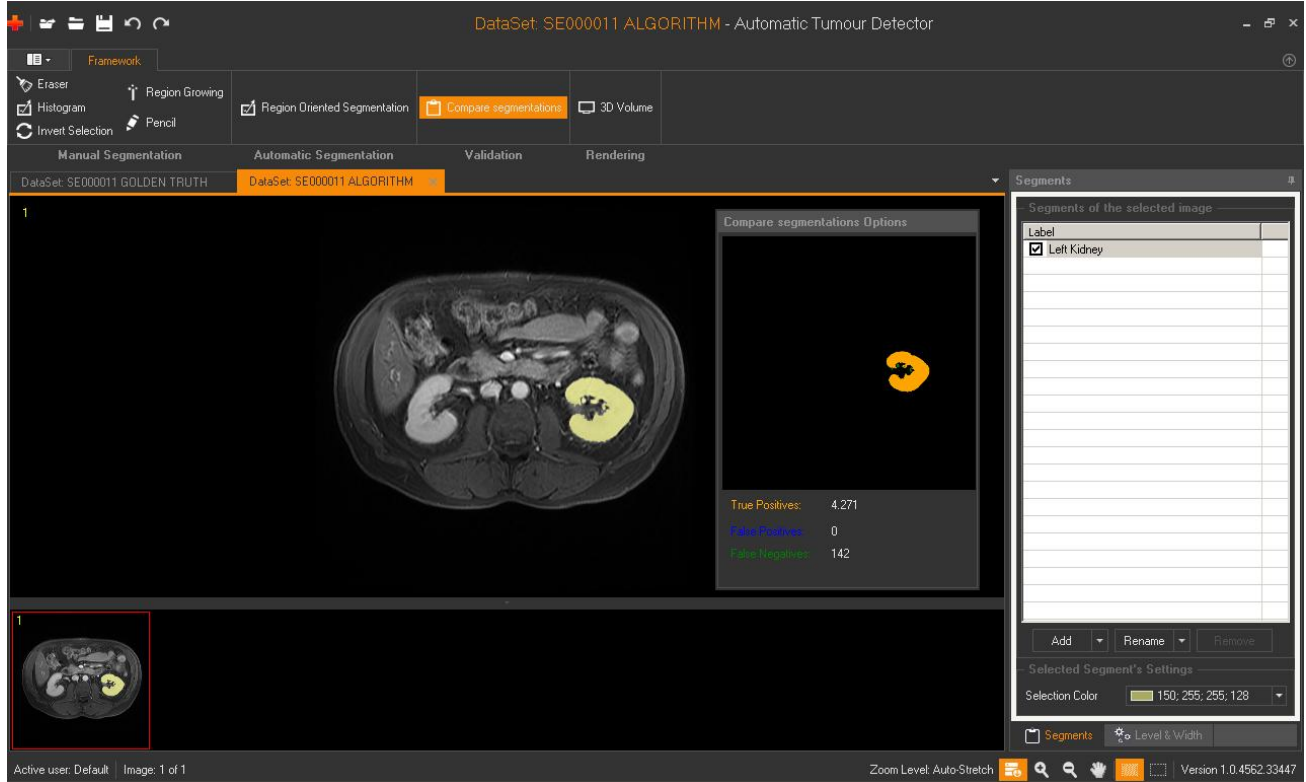

Fig. 2.2: Validation Panel – Single Slide Validation Process

(Clinician's (Golden Truth) vs the medical technician's (Algorithm) delineation)

The medical technician opens the same slide as the clinician's and the medical technician's work and the annotations appear automatically. By pressing the "Compare segmentations" button, a panel appears allowing visual comparison of the previously delineated areas. This panel shows the "True Positives" pixels which are the common pixels in the two methods (orange), the "False Negatives" pixels which are presented only in the clinician's work (blue) and the "False Positives" pixels which are presented only in the second image produced by the automatic method (green).

2.7   3D Rendering process using a Visualisation Toolkit (VTK) Implementation

Once the user has annotated all the regions of interest in the specific image dataset, the "3D Volume" rendering panel (top-middle of Fig. 2.3) provides a 3D view and thus enables the manipulation of the resulting volume model. For this implementation the open source "Visualisation Toolkit" (VTK) (The Visualization Toolkit, 2012), has been deployed; which supports a wide variety of visualisation algorithms in a 3D interactive process. This is called upon by the ATD platform and allows a full 3D representation of the organ along with any defined structural abnormalities within it (Fig. 2.3) providing a realistic view of the area in 3D as well as a quantitative analysis of the medical imaging data.

2.8   Storage Information and wireless transmission

The selected areas in the corresponding medical images are finally saved in external (xml-structured) anonymised files. A typical file size of a complete image dataset is about 500 Kbytes (uncompressed) which enables efficient exchange of such data across remote sites for example for sending them to another expert for a second opinion. Thus the user has the option to e-mail a "Template" to another radiologist, to automatically reveal important findings in seeking a second opinion. A typical size of a "Template" file is about 2 Kbytes.

In the next revision of the system, the capability for transmission of selected compressed images to a mobile device or smartphone will be added. This will allow clinicians to either receive such clinical information or offer opinions while they are on the move.
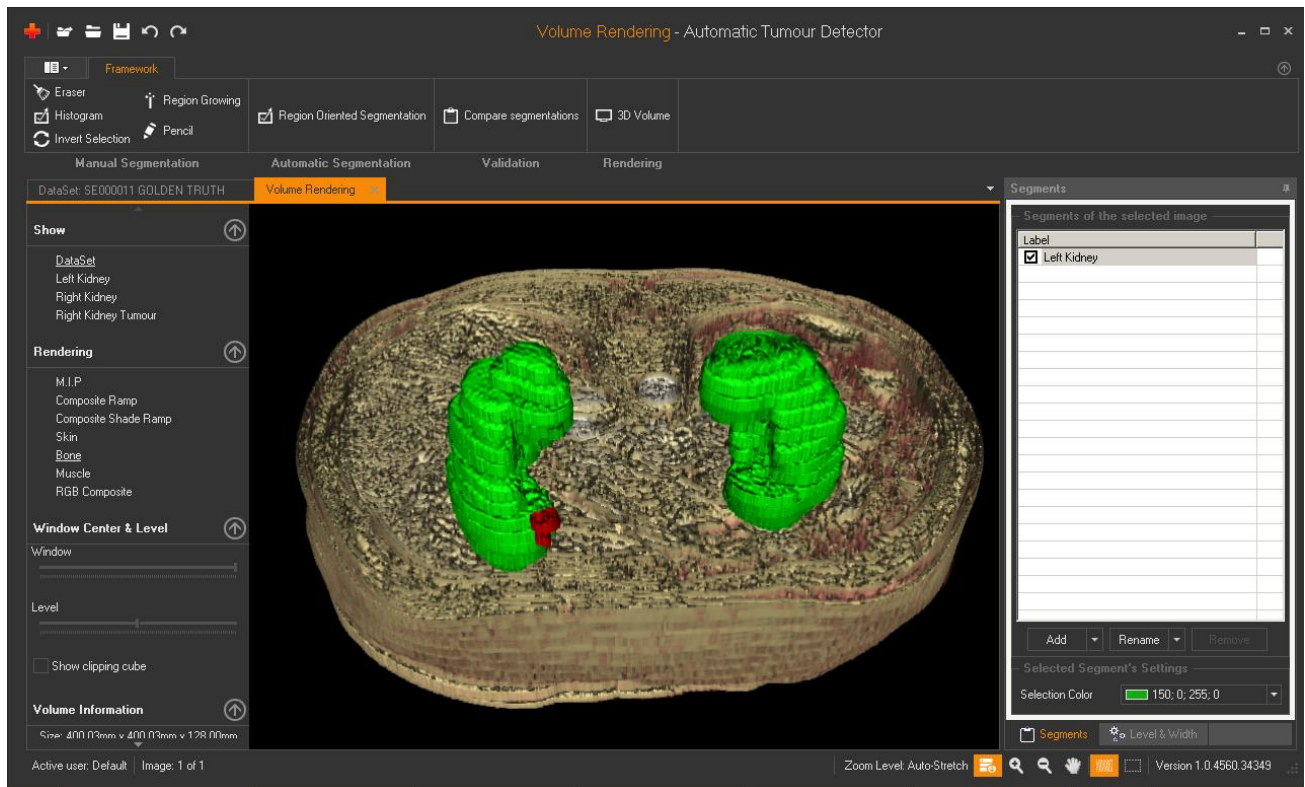

Fig. 2.3: 3D model of the body integrating the previously delineated areas.

Green represents the kidneys while red identifies the tumour.
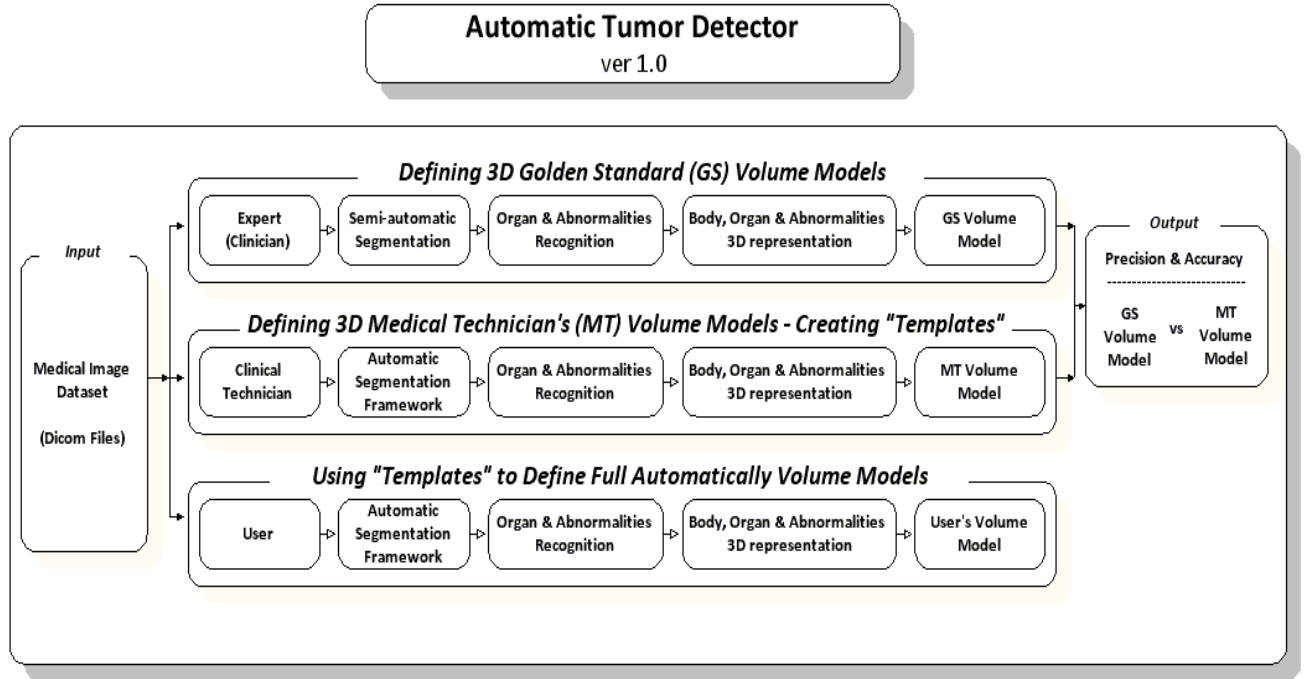
3 EXPERIMENTAL

Fig. 3.1: Methodology used for the for the evaluation of the automatic segmentation Framework

Clinician's (or Golden Standard (GS)) Volume Model vs the Medical Technician's (MT) Volume Model

In the following section the three basic steps describing the process for achieving a fully automatic 3D segmentation of clinical imaging data are described.

1st Step -Defining "3D Golden Standard Models"

In medical image analysis, the main problem is that the outcome must be compared with a baseline (Golden Standard model) in order to validate the performance of the image processing algorithms applied to the dataset. As shown in Fig. 3.1, the process calls for clinicians to identify important areas to be delineated and annotated (e.g. kidneys, tumours, stones and cysts) in the medical image dataset in order to define a "Golden Standard Model" for the evaluation of the outcome in a specific medical image dataset.

Accordingly, the clinician imports a medical dataset into the platform. By using a fast implementation of the "Region Growing" semi-automatic segmentation algorithm and the advanced refinement tools in the "Manual Segmentation" panel, the clinician can accurately define the delineated areas of interest in the images (Fig. 2.1). Once the delineation process has been completed on the image slide where the regions of interest are depicted, the "3D Volume Rendering" option creates a 3D model of the organ structure by integrating the previously delineated areas. By providing a realistic 3D view of the resulting data, this process supports the clinician's attempts to perform an efficient and effective differential diagnosis of possible pathologies in the organ under investigation.

Seven different views of the 3D model are available along with corresponding metrics. They include: M.I.P. (pH-sensitive Molecularly Imprinted Polymer), Composite Ramp, Composite Shade Ramp, Skin, Bone, Muscle and RGB Composite as shown in Fig 3.2 below:
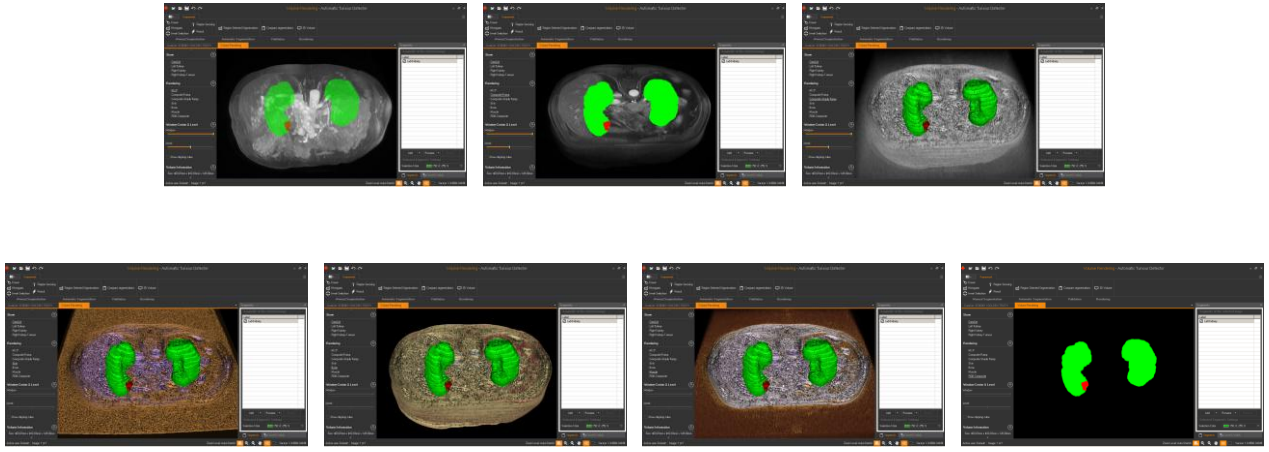
Fig. 3.2: The platform supports seven different views of the 3D models presenting the organs and their abnormalities

(M.I.P., Composite Ramp, Composite Shade Ramp, Skin, Bone, Muscle and RGB Composite)

The initial information presented to the clinician based on the resulting 3D model is exemplified in the table below:

	Body	Left Kidney	Right Kidney	Right Kidney Tumour
X axis (mm)	400,03	84,38	75,00	16,41
Y axis (mm)	400,03	146,88	154,69	18,75
Z axis (mm)	128,00	104,00	112,00	16,00
pixels	4.194.304	46.157	44.415	423
percentage	100,00%	1,10%	1,06%	0,01%

Table 3.1: Metrics resulting from the resulting 3D model; measurements show actual physical sizes of organ structures.

2nd Step -Creating Templates with Rules and Parameters to Identify Specific Areas of Interest

The medical technician uses image slides from the medical image dataset, some of which have been previously delineated and annotated by the clinician, to form rules and parameters to create "Templates". Specifically, by experimenting with the parameters of the "Automatic Region Oriented Segmentation Framework", the medical technician attempts to achieve a segmentation result closest to that of the clinician's (Fig. 3.3). The "Validation" panel allows the evaluation of segmentation results (section 2.6).

Fig. 3.3: Defining parameters and rules ("Templates") for the Automatic Segmentation process

Once the medical technician achieves a result that is very close to the clinician's opinion, it can be stored in a "Template" and can be applied automatically later to a single image or to a series of images (datasets) at once.

3rd Step -Using existing Templates for fully automatic Identification of Specific Areas of Interest

A clinician (or trainee) can import a medical image dataset of the same type as the previous ones (e.g. abdominal images). Using the existing "Templates", the clinician can automatically select a "Template" to apply (e.g. Left Kidney) in order to find a specific organ and view the potential abnormalities in that organ (e.g. Left Kidney, Left Kidney Stone, Left Kidney Tumour).

4 THEORY – THE SEGMENTATION ALGORITHM

4.1 The Region Growing Semi-automatic Segmentation Algorithm

The function of the algorithm is based on finding and demarcating organ structures as a mass of neighbouring pixels in image areas; starting from a single (seed) pixel. It achieves this by examining the intensity levels of the neighbouring pixels and recruiting them as belonging to the structure being grown by spreading the selection outwards starting from a pre-defined (seed) pixel whose grey-level intensity value, plus/minus a so-called "tolerance value", forms the reference value for such recruitment of similar pixels.

The goal in setting the "tolerance value" is to determine how similar in colour a neighbouring pixel must be in order to be selected as belonging to the region being grown. If the tolerance value is relatively low this will result in the algorithm selecting those pixels with colour values near or equal to the reference pixel that is being currently designated as such by the cursor/pointer. Alternatively, high tolerance values would allow a broader range of neighbouring pixels to be included as part of the

region that is being grown (Fujita and Fejri, 2006). In practice, when seeking to demarcate the outer boundaries of the organ image being processed, the choice of the tolerance value can be iteratively adjusted for the best trade-off between selecting too many pixels that, at the next stage, will have to be rejected as irrelevant, or, missing some important pixels that do belong to the organ image being demarcated. To label the delineated organs areas and any abnormalities such as tumours, an image mask (array) is used; this is of the same size as the original image. The pixels in the image mask represent the corresponding positions of the selected pixels in the original image; for enhanced efficiency, the proposed algorithm checks only the pixels that have not already been examined.

Thus the key objective of the Region Growing Methods is the accurate definition of the boundaries of designated areas of interest (e.g. left kidney) (Fig 4.1.1). The fuzzy transition zones which span the tissue boundaries lack colour homogeneity, making the delineation process difficult (Marcotegui and Zanoguera, 2002). To support the clinician in this process, particularly when attempting to delineate complex images, an advanced digital pencil and the eraser tool are integrated with the Region Growing functionality within the platform to automatically keep the similar neighbouring points connected, providing the clinician with the option to swiftly refine their delineations.
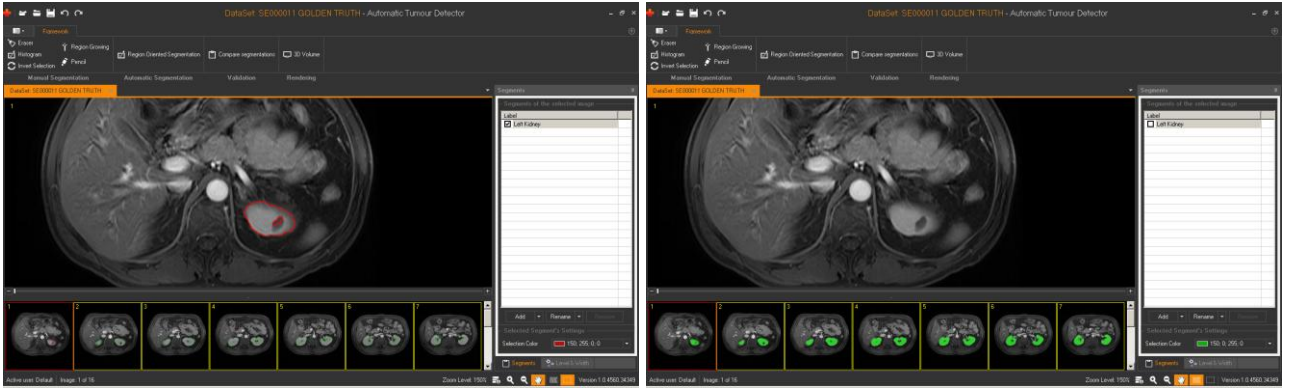

Fig. 4.1.1 Addressing the fuzzy boundaries problem by applying specialised tools

4.2   A Fully Automatic Region Oriented Segmentation Framework

In order to best support the clinical diagnosis process, the proposed Imaging-enabled Assistive Diagnosis system (IAD) has to address the following challenges:

- Locate the clinician's area of interest (e.g. kidney) in the image

- Calculate the average intensity difference of pixel grey-level values within the clinician's area of interest as distinct from the intensity of the surrounding areas

- Initially delineate the structures of interest in the image by simply defining intensity and tolerance values; resolve the delineation and annotation of the area and any abnormalities within it either through using a reference pixel value and iteratively optimised tolerance margins or by following the clinician's delineation and annotation of abnormalities in that area, and finally,

- Accurately describe the delineated areas in detail

The system responds to the above challenges, through the following steps as applied to the recognition of the Kidneys as a demonstrator case.

1st Step – *Pre-processing*

As depicted in Fig.4.2.1 below, the segmentation process starts with a pre-processing procedure using an edge-preserving anisotropic (or Perona–Malik) diffusion filter (Perona and Malik, 1990), so that small image artefacts are smoothed (intra-regional smoothing), whilst objects of interest such as edges are enhanced (inhibiting inter-regional smoothing).
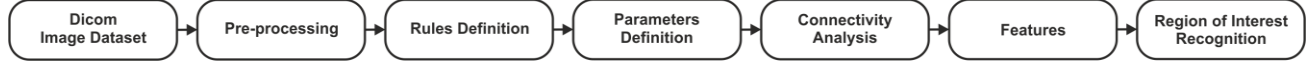

Fig. 4.2.1 The proposed Region-Oriented Segmentation Framework

2nd Step: *Rules Definition*

In clinical practice, the first step towards the recognition of regions of interest is to target their location. The platform gives the clinician the option to define a "working area" in the sequence of images to ensure that it includes the targeted objects (e.g. in our demonstrator case this is Kidneys). Defined "working areas" are stored in "Templates" and can be used in the identification of specific objects in a given medical image dataset. This avoids false positives and minimises the amount of information which needs to be processed.

3rd Step: *Parameters Definition*

Generally, a histogram displays the frequency of the grey-levels in an image. If there exists no user-specified region of interest as a working area where the organ is located, the automatic process would typically result in a larger area being designated as the region of interest. To resolve this, in this step the system deploys a modified algorithm as introduced by H. Bassman and P. Besslich (1995). In the equation below (Eq.4.2.1), $h(gv)$ is the histogram value for a specific grey-scale value gv, *Max* is the maximum value of the histogram and *NormMax* is the normalised maximum value defined by the user.

$$h(gv) = \text{int}((float)h(gv) * NormMax / Max) \qquad \text{Eq. (4.2.1)}$$

A normalisation of the histogram process through the right definition of the associated NormMax parameter is required to avoid problems in the next step due to overflow events.

To identify the abnormalities located in a designated area, the dynamic range of the histogram entries has to be compressed in such a way that the lower entries of the histogram are emphasised. This is achieved by using Equation (4.2.2).

$$h(gv) = 10\sqrt{h(gv)} \qquad \text{Eq. (4.2.2)}$$

In this way, small peaks in the histogram corresponding to small areas in the image are emphasised, allowing the algorithm to detect them more accurately.

As a starting point, a process of smoothing the histogram must be applied to homogenise and successfully detect relatively large areas (organs) avoiding the insignificant local peaks (i.e. variations in colour inside the organ image area). The histogram is smoothed by applying the computational method whereby all the intensity values of the pixels in the image are re-calculated by determining the average of a pre-defined number (the link "Width") of neighbouring pixels of the histogram. This interpolation "width" parameter is defined experimentally by the user, supported by real-time visualisations (Fig. 3.3). The higher width values are associated with larger areas being designated as part of the organ structure of interest; while low width values help the user pick out the smaller

structures thus attempting to avoid missing any important parts of the image. If the Width parameter is set to 1 the smoothing process is disabled.

By detecting the falling and rising histogram edges one can determine the number of valleys in the histogram, thus inferring the threshold values.
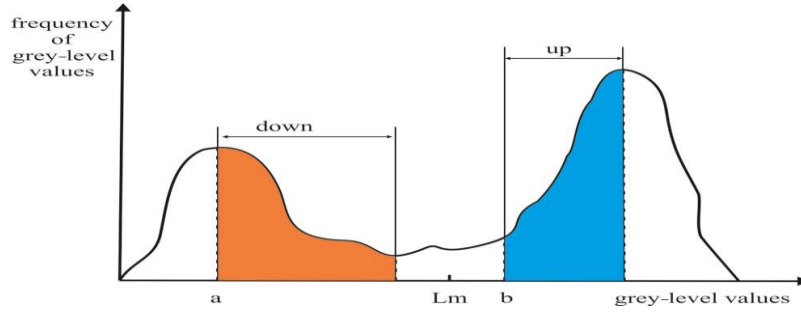

Fig. 4.2.2 Automatic definition of thresholds (Lm) process (Eq. 4.2.3)

A "Threshold" (Lm) is defined as:

$$Lm = a + down + [b - (a + down)]/2 \qquad \text{Eq. (4.2.3)}$$

In this equation, a represents a local maximum value and b is the point where the histogram starts to rise again (ignoring any small peaks under a predefined limit value). These local minimum values (Lm) are used to segment objects and to create a "Label Image" (Fig 4.2.3). In this figure, two thresholds are used (Lm1=0, Lm2=5) to identify two different zones. For example, the left Kidney in Fig. 4.1.1 corresponds to the second curve in the histogram (Fig. 4.2.2). The closer the peak of this curve is to Lm, the more the delineated boundary moves inwards towards the centre of the kidney.

The platform provides the clinician with the option to define the "up" and "down" parameters which are also stored in the "Templates" in order to achieve the desired Lm values in complex images.

Applying any filter to an image introduces a certain amount of noise. This noise can be removed by using erosion-dilation linear morphological filters. By applying a 3x3 erosion filter, the user defines a "Threshold" (i.e. the number of the neighbouring pixels, max 8 in a 3x3 mask), whereby a value of "0" removes the central pixel of the 3x3 mask. Conversely, using the dilation filter the user defines a "Threshold" to place a pixel at the central position of the 3x3 mask with an intensity corresponding to the same colour value of the mask region.

4th Step: *Connectivity Analysis*

In order to create the final "Mark Image" which depicts the regions of interest, L-shape masks are used (based on the 6-connected neighbourhood technique) (Horn, 1986) to compare the label value of every pixel to the values of the neighbouring pixels. The pixels with the same values in the "Label Image" but different values in the "Initial Image" are included in the list of pixels to be considered later when identifying the number of the different objects in the image.

Initial Image

1	1	1	0	7	7
1	1	1	0	7	7
1	1	1	0	7	7
4	4	7	7	7	7
4	4	7	7	7	7
4	4	4	4	7	7

Label Image

1	1	1	0	2	2
1	1	1	0	2	2
1	1	1	0	2	2
1	1	2	2	2	2
1	1	2	2	2	2
1	1	1	1	2	2

Mark Image

a	a	a	-	c	c
a	a	a	-	c	c
a	a	a	-	c	c
b	b	c	c	c	c
b	b	c	c	c	c
b	b	b	b	c	c

Fig. 4.2.3 Automatic identification of objects using L-shaped masks (3 Objects a, b and c are identified)

In this example (Fig 4.2.3), the "Mark Image" contains 4 identified regions. This is based on the work of Bassmann and Besslich (1995) which sets out this method in detail.

Thus the modifications applied to the "Fully Automatic Region Oriented Segmentation Framework" include the addition of a pre-processing procedure (Perona–Malik diffusion filter), (Eq. 4.2.2) to emphasise the details of the current type of images (e.g. abdominal), an implementation of an L-shape mask based on the 6-connected neighbourhood pixels in the Connectivity Analysis (CA) process, and a top-down connectivity analysis of the detected regions. The CA method requires at least one common point between one image slide and the next so as to verify the region boundary. Moreover, the average intensity of the grey-level values of the selected region is calculated and a tolerance value is defined. This criterion must also apply to every following image slide in order to successfully detect the desired region.

5th Step*: Features*

The above-mentioned "Region-Oriented Segmentation Framework" applied to an CT/MRI image dataset can delineate regions of interest which can be categorised based on features such as the compactness, the centre of gravity (the central point of a defined area), total area (number of the pixels) and the perimeter of a specific region. The compactness or density and the centre of gravity are features that are independent of the exact position, rotation and scaling of the object, so they are very useful in the identification process.

The current version of the IADS system additionally stores another two parameters from the above-mentioned features in the "Template" file. Firstly the "total area" which is a criterion to be considered for objects of interest so as to avoid erroneously detecting very small objects during the organ image identification and delineation process, and secondly, the "centre of gravity" of an object which must be located in the working area and must encompass all the pixels of the object.

Finally, the medical technician in creating the "Templates" can click only once on a designated object image (e.g. kidney) from the initially produced list, to obtain the average grey-level value of that object. To avoid selection of other objects with similar intensities, this value is also stored in the "Template" with an additional tolerance value as can be defined by the medical technician.

For the recognition of kidney abnormalities (tumours, stones and cysts), some statistical data can be additionally considered to arrive at the threshold values for the average grey-level intensity typical of

some structures representing abnormal or pathological changes e.g. cysts.

Cysts are relatively dark; tumours are grey, while stones have relatively higher grey-level values. The "Analysis" panel (Fig. 4.2.4) enables the medical technician to experiment with defining the three parameters for the identification of any of the above-mentioned abnormalities/pathologies consistent with the clinician's judgment.

The first parameter refers to the grey-level "Value" that the pixels of an object (e.g. a pixel in an image of an abnormal kidney structure) is typically expected to have to be designated as such i.e. recognised e.g. as a stone, a tumour or a cyst. Due to the non-homogenous distribution of grey-level values of the pixels in the MRI images of such organs, a "Tolerance" value must also be defined so that "grey-level Value ± Tolerance" corresponds to the range of intensities of pixel values typically expected to depict such abnormal structures. In this way, pixels which meet the above criteria (potential seeds) are obtained. However, this methodology can also erroneously designate a number of irrelevant pixels with similar intensities scattered in the organ image (classification noise). In order to identify only the best candidate seeds corresponding to the abnormalities and thus minimise the classification noise, a 9 x 9 erosion filter is used. Here, the medical technician must declare the number of neighbourhood pixels (threshold) to be taken into account (Maximum 9 x 9 = 81 neighbourhood pixels). Finally, the best candidate seeds with intensity levels closest to the respective thresholds are used in a filling process (region growing) to fill up and this helps to demarcate the sub-structural areas which represent the kidney abnormalities.
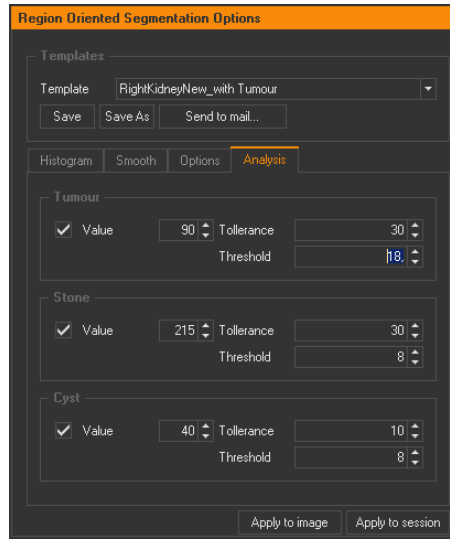
Fig. 4.2.4 Creating "Templates" for an automatic identification of kidney abnormalities (tumours, stones and cysts)

5   RESULTS

Evaluation of the "Automatic Segmentation Framework" is based on the following five criteria (Mahalakshmi et al., 2009): Accuracy, Precision, Sensitivity, Specificity and Dice Similarity Coefficient. These metrics provide a means of benchmarking of performance of IADS. Generally, pixels are classified into four categories: True Positives (Correctly Selected), True Negatives (Correctly Rejected), False Positives (Mistakenly Selected), and False Negatives (Mistakenly Rejected). The numbers of these pixel categories can be used in the following formulae to calculate the values of the above metrics.

"Accuracy" is the proportion of true results ("True Positives" and "True Negatives") in the population of the results; as shown in Eq. (5.1) below:

$$Accuracy = \frac{TruePositives + TrueNegatives}{TruePositives + TrueNegatives + FalsePositives + FalseNegatives} \quad \text{Eq. (5.1)}$$

"Precision" is defined as the proportion of "True Positives" against all the positive results ("True Positives" and "False Positives"); as shown in Eq. (5.2) below:

$$Precision = \frac{TruePositives}{TruePositives + FalsePositives} \quad \text{Eq. (5.2)}$$

"Sensitivity" refers to the ability of the system to identify positive results. In other words, it measures the proportion of positives which are correctly identified as such; this is shown in Eq. (5.3) below:

$$Sensitivity = \frac{TruePositives}{TruePositives + FalseNegatives} \quad \text{Eq. (5.3)}$$

"Specificity" refers to the ability of the system to identify negative results, which means that it measures the proportion of negatives correctly identified as such; this is shown in Eq. (5.4) below:

$$Specificity = \frac{TrueNegatives}{TrueNegatives + FalsePositives} \quad \text{Eq. (5.4)}$$

"Dice Similarity Coefficient" (DSC), defines the similarity measure over two 3D volume models; as shown in Eq. (5.5) below:

$$DSC(GS, CT) = \frac{2|GS \cap MT|}{|GS| + |MT|} \quad \text{Eq. (5.5)}$$

Where GS is the Clinician's volume model (Golden Standard) and MT is the Medical Technician's volume model (Automatic Segmentation Framework).

As an example, after applying equations 5.1, 5.2, 5.3, 5.4 & 5.5 to the SE00004 MRI dataset, we have obtained the following results:
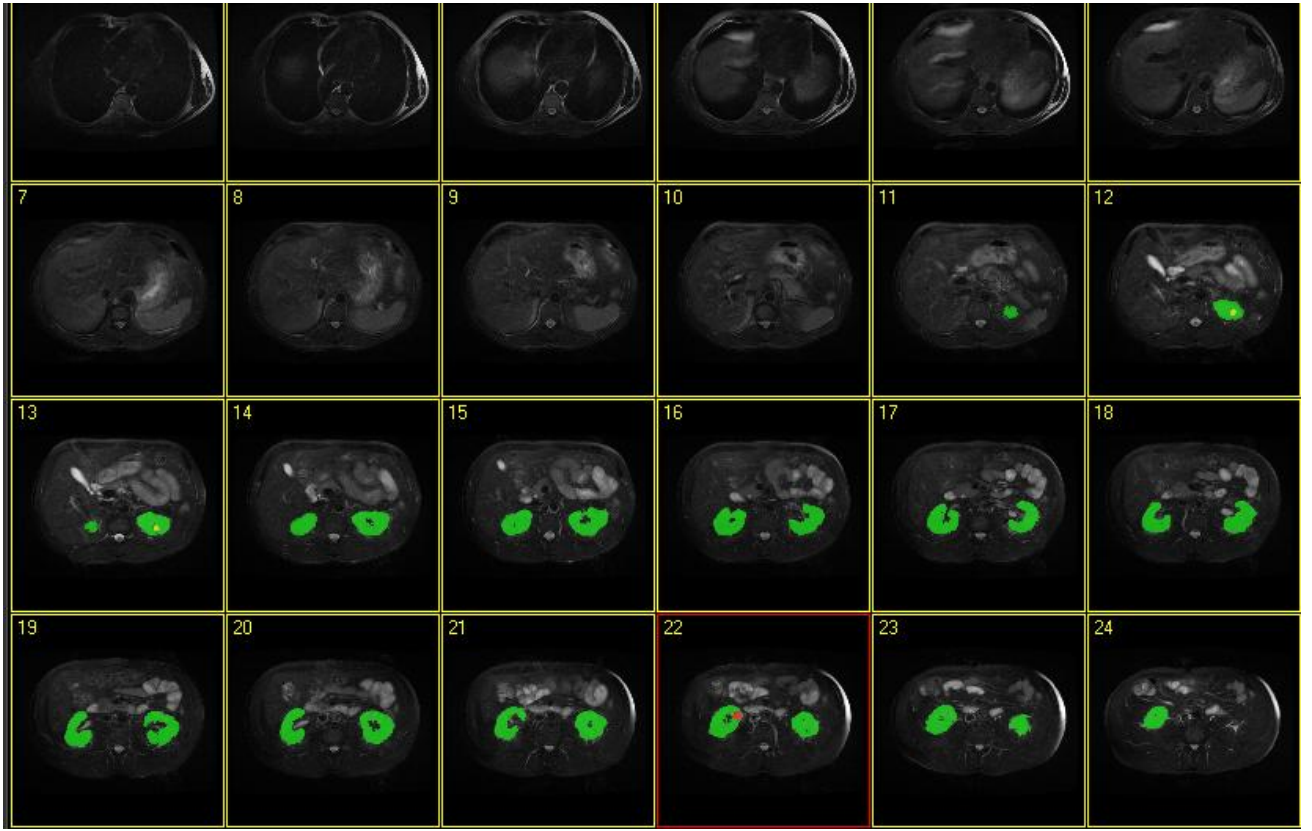
Fig. 5.1 Automatic identification of objects (e.g. Left Kidney, Right Kidney, Right Kidney Tumour (No 22 slide) & Left Kidney Stone (No 12 & No 13 slides) – SE00004 MRI dataset)

a/a	SE000004 MRI Dataset	True Positives (Correctly Selected)	True Negatives (Correctly Rejected)	False Positives (Mistakenly Selected)	False Negatives (Mistakenly Rejected)	Accuracy	Precision	Sensitivity	Specificity	Dice similarity
1	MR000000	0	262.144	0	0					
2	MR000001	0	262.144	0	0					
3	MR000002	0	262.144	0	0					
4	MR000003	0	262.144	0	0					
5	MR000004	0	262.144	0	0					
6	MR000005	0	262.144	0	0					
7	MR000006	0	262.144	0	0					
8	MR000007	0	262.144	0	0					
9	MR000008	0	262.144	0	0					
10	MR000009	0	262.144	0	0					
11	MR000010	651	261.493	47	43	99,97%	93,27%	93,80%	99,98%	93,53%
12	MR000011	2.238	259.906	26	118	99,95%	98,85%	94,99%	99,99%	96,88%
13	MR000012	3.254	258.890	12	258	99,90%	99,63%	92,65%	100,00%	96,02%
14	MR000013	4.225	257.919	72	120	99,93%	98,32%	97,24%	99,97%	97,78%
15	MR000014	3.954	258.190	8	208	99,92%	99,80%	95,00%	100,00%	97,34%
16	MR000015	3.727	258.417	21	201	99,92%	99,44%	94,88%	99,99%	97,11%
17	MR000016	3.472	258.672	13	108	99,95%	99,63%	96,98%	99,99%	98,29%
18	MR000017	3.603	258.541	32	239	99,90%	99,12%	93,78%	99,99%	96,38%
19	MR000018	4.250	257.894	112	160	99,90%	97,43%	96,37%	99,96%	96,90%
20	MR000019	4.408	257.736	148	107	99,90%	96,75%	97,63%	99,94%	97,19%
21	MR000020	4.018	258.126	120	91	99,92%	97,10%	97,79%	99,95%	97,44%
22	MR000021	3.021	259.123	109	53	99,94%	96,52%	98,28%	99,96%	97,39%
23	MR000022	1.850	260.294	115	74	99,93%	94,15%	96,15%	99,96%	95,14%
24	MR000023	0	262.144	0	0					
					Average	99,92%	97,69%	95,81%	99,98%	96,72%

Table 5.1: Accuracy and precision of the delineation of the Left Kidney (SE000004 MRI dataset)

a/a	SE000004 MRI Dataset	True Positives (Correctly Selected)	True Negatives (Correctly Rejected)	False Positives (Mistakenly Selected)	False Negatives (Mistakenly Rejected)	Accuracy	Precision	Sensitivity	Specificity	Dice similarity
22	MR000021	349	262.144	26	0	99,99%	93,07%	100,00%	99,99%	96,41%
					Average	99,99%	93,07%	100,00%	99,99%	96,41%

Table 5.2: Accuracy and precision of the delineation of the Left Kidney Tumour (SE000004 MRI dataset)

a/a	SE000004 MRI Dataset	True Positives (Correctly Selected)	True Negatives (Correctly Rejected)	False Positives (Mistakenly Selected)	False Negatives (Mistakenly Rejected)	Accuracy	Precision	Sensitivity	Specificity	Dice similarity
12	MR000011	184	262.144	13	0	100,00%	93,40%	100,00%	100,00%	96,59%
13	MR000012	171	262.144	9	0	100,00%	95,00%	100,00%	100,00%	97,44%
					Average	100,00%	93,40%	100,00%	100,00%	96,59%

Table 5.3: Accuracy and precision of the delineation of the Left Kidney Stone (SE000004 MRI dataset)

6   DISCUSSION

Overall, this IAD system has performed as a multi-functional system with the following features as evaluated against CT/MRI-image datasets showing its capability to support clinical diagnosis; specifically with a demonstrator case focusing on assisting in diagnosis of kidney pathologies.

- A multi-functional easy-to-use annotation system

- The ability for real-time detection of kidneys and their abnormalities (i.e. tumours, stones and cysts – if any present)

- A multi-functional 3D visualisation system providing actual geometry (real physical sizes) measurements

- Evaluation of the results based on a 3D volumetric evaluation, as well as on five other measurement methods.

After initial development, the system was tested by clinicians and their feedback was used to improve the usability of the system. Generally, the clinicians commented favourably on the speed and accuracy of the system, as well as on its large variety of functions with an emphasis on the 3D view. A notable shared view expressed by the clinicians was that given that the system was able to recognise kidneys and any abnormal tissue located within them, it should be possible for it to also detect any abnormal tissue that may also be present in the surrounding areas as this is what the clinician would want to examine particularly if there is already clinical evidence of abnormal tissue within the organ. This function is being currently integrated whilst the system is undergoing a large clinical trial to include at least 100 MRI datasets of an average of 25 slides each.

Since the input of the system is CT/MRI datasets, it follows that these must be produced by well calibrated CT/MRI scanners in order to ensure maximum effectiveness.

Results have shown that currently the system is able to accurately detect "relatively compact" regions such as stones, cysts and tumours. In more complex cases where, for example, a tumour has spread into different areas with varying intensities, the system can recognise the tumours but with decreased accuracy; this is being addressed through a set of more advanced algorithmic approaches.

Finally, care was taken to ensure that the output files were anonymised and were also of a small size and thus easier to download by clinicians over the clinic network. This would also enable the system to securely and efficiently transmit files, including images, to client applications running on smartphones (Windows or Android) so that, clinicians and consultants could view the results, on the move, as and when required to save time and increases the diagnostic accuracy through second opinions.

7 CONCLUSION

This research has resulted in the development and evaluation of a CT/MRI Imaging Diagnosis Assistive (IAD) system for abnormality detection and delineation as may be present in any organ structures under examination. A demonstrator for kidney diagnosis; providing full 3D automated identification of kidneys and their abnormalities (tumours, stones and cysts) has been configured and clinically evaluated. The IAD has integrated two methods to create "3D Volume Models" from MRI datasets. The first method provides support, through an intuitively user interface, for clinicians to rapidly identify and delineate areas of interest, with a 3D view and have real metrics at hand specifying actual physical sizes of organ structures and any abnormal tissue regions. The second method invokes a fully 3D automatic way to identify important areas based on "Templates" initially created by, for example, a medical technician and later on used by clinicians with no prior knowledge of medical image segmentation. These "Templates" allow the system to identify organ structures based on their features and look for any abnormalities. Clinicians who participated in the trials expressed satisfaction with this semi-automatic method in that it offered better visualisation of regions of interest, as it simplified and sped up the image annotation process even in very complex medical image datasets enabling higher accuracy organ and abnormality identification. As using the system requires no previous knowledge of auto-labelling, it is easy to use to support the clinical diagnosis process throughout; from the input stage of the CT/MRI image datasets to the generation of 3D models; its Automatic Segmentation Framework has been tested on 11 MRI datasets (286 Images). Benchmarking tests of the system have shown promising results. For the recognition of kidneys and their abnormalities, the system outperformed previously reported results with a mean DSC of 97% and 96% respectively compared to other systems with a mean DSC 95% and 91% at best. Future developments of the system will include a collection of "Templates" to be used in the recognition of other organs and their associated abnormalities (e.g. brain, spine, knees, etc.).

REFERENCES

Akbari H., Fei B. 2012. Automatic 3D Segmentation of the Kidney in MR Images Using Wavelet Feature Extraction and Probability Shape Model. Proceedings of SPIE 2012, Vol. 8314, Medical Imaging 2012: Image Processing, pp. 83143D1-83143D7. Doi: 10.1117/12.912028.

Bassman H., Besslich P.W., 1995. Ad Oculos – Digital Image Processing – Student Version 2.0, ISBN 1-85032-132-9, pp. 117-152.

Benefits of the Microsoft .NET Framework [Online]. Available at: http://msdn.microsoft.com/en-us/kb/kbarticle.aspx?id=829019 [2012]

Campadelli P. et al., 2008. Fully Automatic Segmentation of Abdominal Organs from CT images Using Fast Marching Methods. 21st IEEE International Symposium on Computer-Based Medical Systems (CBMS 2008), pp. 554-559.

Chen X. et al., 2011. FEM-Based 3-D Tumour Growth Prediction for Kidney Tumour, IEEE Transactions on Biomedical Engineering (2011), Vol. 58, No 3, March 2011, pp. 463-467. Doi: 10.1109/TBME.2010.2089522.

Fujita H., Fejri M., 2006. New trends in software methodologies, tools and techniques: How to create the magic wand? Proceedings of the Fifth SoMeT-06, IOS press. ISBN 1-58603-673-4, pp. 127-132.

Gloger O. et al., 2012. Prior Shape Level Set Segmentation on Multistep Generated Probability Maps of MR Datasets for Fully Automatic Kidney Parenchyma Volumetry. IEEE Transactions on Medical Imaging, Vol. 31, No. 2. pp. 312-325. Doi: 10.1109/TMI.2011.2168609.

Horn B.K.P, 1986. Robot vision. Cambridge, London: MIT Press. ISBN 0-262-08159-8.

Hu X. et al., 2004. Independent analysis of four-phase abdominal CT images. Proceedings of MICCAI 2004, LNCS 3217, pp. 916-924. Doi: 10.1007/978-3-540-30136-3_111.

Kim D., Park J., 2004. Computer-aided detection of kidney tumour on abdominal computed tomography scans. Acta Radiologica (2004), Vol. 45, No. 7, pp 791-795. Doi: 10.1080/02841850410001312.

Li K., Fei B., 2008. A New 3D Model-based Minimal Path Segmentation Method for Kidney MR Images. The 2nd International Conference on Bioinformatics and Biomedical Engineering, ICBBE 2008, pp. 2342 – 2344. Doi: 10.1109/ICBBE.2008.918.

Lin D-T. et al, 2006. Computer-Aided Kidney Segmentation on Abdominal CT Images. IEEE Transactions on Information Technology in Biomedicine, Vol. 10, No 1, pp. 59-65. Doi: 10.1109/TITB.2005.855561.

Mahalakshmi T. et al., 2009. Connectivity Characteristic of Transcription Factor. World Academy of Science Engineering and Technology (WASET), International Journal of Information and Communication Engineering, Vol. 5, No 7, pp. 471-474.

Marcotegui B., Zanoguera F., 2002. Image editing tools based on multi-scale segmentation. In H. Talbot and R. Beare (eds.), Mathematical Morphology VI, (Proc. ISMM02, Sydney, Australia, April 2002). CSIRO, pp. 127-135.

Park H. et al., 2003. Construction of an abdominal probabilistic atlas and its application in segmentation. IEEE Transactions on Medical Imaging, Vol. 22, No 4, (April 2003), pp. 483-492. Doi: 10.1109/TMI.2003.809139.

Perona P., Malik J., 1990. Scale-space and edge detection using anisotropic diffusion. IEEE Transactions on Pattern Analysis and Machine Intelligence, Vol. 12, No 7, pp. 629-639. Doi: 10.1109/34.56205.

Prevost R. et al., 2012. Kidney detection and real-time segmentation in 3D contrast-enhanced ultrasound images. 9th IEEE International Symposium on Biomedical Imaging (ISBI 2012), Barcelone, Spain, pp. 1559-1562. Doi: 10.1109/ISBI.2012.6235871.

Rao M. et al, 2005. Comparison of human and automatic segmentations of kidneys from CT images. International Journal of Radiation Oncology, Biology, Physics, Vol. 61, No 3, (March 2005), pp. 954–960. Doi: 10.1016/j.ijrobp.2004.11.014.

Sakashita M. et al., 2007. A method for extracting multi-organ from four-phase contrasted CT images based on CT value distribution estimation using EM-algorithm. Medical Imaging 2007, Computer-Aided Diagnosis, Proceedings of the SPIE, Vol. 6514, pp. 65141C. Doi:10.1117/12.709232.

Shimizu A. et al., 2006. Multi-organ segmentation in three dimensional abdominal CT images. International Journal of Computer Assisted Radiology and Surgery (CARS), Vol. 1, SUPP/1, pp. 76-77. ISSN 1861-6410.

The Mono project [Online]. Available: http://www.mono-project.com/Main_Page [2012]

The Visualization Toolkit (VTK) [Online]. Available: http://www.vtk.org/ [2012]

Yao C. et al., 2006. Simultaneous location detection of multi-organ by atlas-guided eigen-organ method in volumetric medical images. International Journal of Computer Assisted Radiology and Surgery (CARS), Vol. 1, SUPP/1, pp. 42-44. ISSN 1861-6410.

Emmanouil Skounakis is a PhD Candidate at Brunel University. He holds two M.Sc. degrees in Data Communication Systems and in Electronic and Computer Engineering with a focus on Biomedical Imaging. He currently lectures Informatics at the Technological Educational Institute of Crete. He has several publications in International Journals and Conferences in the field of Image Processing, with applications in Biomedicine, Automatic Control Systems and Geophysics. He has participated in several research projects and he is a reviewer for the IEEE Engineering in Medicine and Biology Society.

Dr. Konstantinos Banitsas Konstantinos Banitsas has a B.Sc. in Computer Science (1993), an M.Sc. in Electronic engineering (1997) and a Ph.D. in Telemedicine (2004). He also holds an MA in Higher Education (2011). He is currently working as a lecturer at Brunel University (UK) and is the director of studies for the computer systems engineering course. His research focuses on e-Health, Telemedicine and wireless communications where he has published more than 30 papers in International Journals and Conferences. He is a member of the IEEE and the IET.

Dr. Atta Badii is a high ranking professor (Chair of Secure Pervasive Technologies) at the University of Reading. His various leadership roles include: Founding Director of the Intelligent Systems Research Laboratory, Chairman of the Steering Board of the European Research NoE in Video-Analytics, Chair of Security Architectures and Virtualisation Paradigms for the European SecurIST Research Roadmap Programme, Founding Chair of The Trustworthy Internet of People, Things and Services SIG, Founding Chair of the Companion Robotics Institute, Member of the Board of the UK Academy of Information Systems, Founding Chair of the UKAIS (Midlands), Chairman of the Board of the East Midlands Telematics Development Trust, Director of the ETDT Media Technologies Research Group

M.D. Stavros Tzoulakis received his Medical degree as a Surgeon Urologist from the Faculty of Medicine - University of Crete, Greece.
He is with the Venizeleion General Hospital of Heraklion (Crete), where he is working as a Clinical Surgeon Urologist.
He also lectures at the Medical School at the University of Crete. His research interests include the study of urinary cancer and pathology of the urinary system.
He has several publications in International Journals and Conferences in the field of urinary pathology.

Dr. Emmanuel Maravelakis is an Assistant Professor and the head of the Design and Manufacturing Laboratory of the Technological Educational Institute of Crete. He is the scientific coordinator in 7 research projects with a total of 0,5M euros in funding and he has also participated as main researcher in 19 others national & European projects. His publications include (1) Book in "CAD/CAM systems & 3D modeling" and several international Journal and Conferences. His research interest focuses on CAD/CAM systems, 3D Modeling, Reverse Engineering, New Product Development and Bioengineering.

Dr. Anthony J. Konstantaras is an Assistant Professor in Software Engineering at the Department of Electronics of the Technological Educational Institute of Crete and Head of Sector of Computing and Control. His research interests invoke areas of Software Engineering, such as Intelligent Systems and Soft Computing, with various signal and image processing applications in medicine, geophysics and astrophysics, as well as the design, development and implementation of parallel processing algorithms for the aforementioned systems. Dr. A. J. Konstantaras serves as reviewer for the I.E.E.E. journals Fuzzy Systems, Selected Topics in Geophysics and Remote Sensing, and Geosciences and Remote Sensing Letters.

21